Scientia Iranica B (2023) 30(1), 1–15

SCIENTIA IRANICA

Sharif University of Technology
Scientia Iranica
Transactions B: Mechanical Engineering
http://scientiairanica.sharif.edu

Mechanical properties, microstructure, and fracture behavior of friction stir welded AA7075 joints with conical pin and conical threaded pin type tools

V.S. Gaikwad* **and S. Chinchanikar**

Department of Mechanical Engineering, Vishwakarma Institute of Information Technology, Pune, Maharashtra State, 411048, India.

Received 14 October 2021; received in revised form 24 May 2022; accepted 15 August 2022

KEYWORDS
FSW;
AA7075;
Microhardness;
Tensile strength;
Microstructure analysis;
Scanning electron microscopy.

Abstract. This study investigates the mechanical properties, microstructure, and fracture behavior of Friction Stir Welded (FSWed) AA7075 joints considering the influence of process parameters and tool geometry. FSWed joints are produced with a conical pin and conical threaded pin type tools using tool rotational speeds of 1400 and 2000 rpm and welding speeds of 20 and 40 mm/min. The FSWed joint showed higher values of the tensile strength (188 MPa), percentage elongation (5.7%), and microhardness (137 HV) with the conical threaded pin type tool. However, the conical pin type tool produced a minimum surface roughness of 9.59 μm. A comparatively lower tensile strength observed for the FSWed joint with a conical pin type tool could be attributed to their coarser, elongated, and heterogeneous grain distribution and porosity defects in the welding zone. No significant difference was observed in the microhardness for the conical pin and conical threaded pin type tools. The fracture of the FSWed joint predominantly occurred in the heat-affected zone during the tensile test. The FSWed joint produced with a conical threaded pin had better mechanical properties, favorable microstructure, and ductile type fracture behavior at a welding speed of 40 mm/min and a tool rotation of 2000 rpm.

1. Introduction

AA7075 aluminum alloy with its low density and better mechanical properties finds wide applications in the defense, aerospace, military, and automotive sectors. Friction Stir Welding (FSW) is preferred to join aluminum alloys due to liquation cracking and solidification observed with fusion welding [1]. FSW being a low heat input process produces joints with better mechanical properties, low residual stresses, porosity, distortion, and brittle dendrite structure against the fusion-welded joints [2,3]. The microstructure of Friction Stir Welded (FSWed) joints shows equiaxed and fine grains (1.5–3.7 μm) in the Weld Nugget (WN) [4].

A group of researchers observed significant variation in the microstructure and mechanical properties of FSWed AA7075 aluminum alloy joints with the tool rotation [5–7]. Almost all studies reported variations in the grain size and shear textures in the WN with the tool rotation and fracture of the FSWed joints in the lowest hardness zone after the tensile tests. Most studies observed narrower, stronger Heat-Affected Zones (HAZs) and higher hardness in the nugget zones at higher welding speeds. Further, studies found the material flow direction in the nugget zone leaning towards the welding direction with increase in the welding speed. The corrosion resistance of the FSWed AA7075 aluminum alloy joints was also reportedly varying with

*. *Corresponding author. Tel.: +91 9096239959*
E-mail address: vaibhav.219p0007@viit.ac.in (V.S. Gaikwad)

doi: 10.24200/sci.2022.59154.6087

respect to the welding speed and was found to be minimum at a tool rotational speed of 1000 rpm [8].

FSW of AA7075-T651 aluminum alloy with forced (water or compressed air) cooling increased the yield point of the joint and shifted fracture location from the HAZ to an intermediate region between the WN and Thermo-Mechanically Affected Zone (TMAZ) [9]. The effect of temper conditions on the friction-stir weldability of AA7075 Al-alloy plates was also reported [10]. The joints produced in the T6-temper conditions exhibited lower strength values than the base plate. However, strength values observed were comparable to the base plate for the joints produced in the O-temper condition.

The microhardness of FSWed of similar and dissimilar aluminum alloy joints exhibited variation in the welding zone, mostly the following distribution of a letter 'W' shape, and found a minimum value at the interface of WN and TMAZ [11–14]. Most studies illustrated the recrystallization of grains at WN and fracture of the FSWed joints at the interface of TMAZ and HAZ during the tensile test. The tool force and surface roughness were significantly affected by tool rotation and welding speed. The lowest surface roughness was reported as 3.61 μm at a tool rotation speed of 960 rpm and a welding speed of 45 mm/min [15]. Efforts were also made to investigate the effect of post-weld heat treatment and the addition of boron carbide in WN on microstructure and pitting corrosion of FSWed joints of AA7075 aluminum alloy. A significant improvement in pitting corrosion resistance was observed with the addition of boron carbide powder and post-weld heat treatment. However, studies found a slight decrease in the hardness [16].

The tool geometry significantly affects the mechanical properties and microstructure of FSWed joints [17–21]. Mastanaiah et al. [18] observed better mechanical properties and consistent material flow during FSW of AA2219-T6 plates with a hybrid tool pin profile against the conical tool. Amirafshar and Pouraliakbar [19] found better mechanical properties and wear resistance for FSWed structural steel joints with the square pin tool than cylindrical, conical, and triangular tools. Beygi et al. [20] determined a better material flow and tensile strength for FSWed Al-Cu bimetals with the threaded conical pin. This could be attributed to a larger contact area of the pin which led to higher plasticized material flow. Kumar et al. [21] observed better tensile strength and lower defects in the weld when using a shoulder diameter of 20 mm and a pin diameter of 6 mm. However, lower tensile strength and higher degree of defects were observed with a tool having a shoulder diameter of 10 mm and a pin diameter of 3 mm.

Banik et al. [22] achieved better mechanical properties, higher efficient torque, and force behavior with the taper threaded tool during the FSW of AA6061-T6. A group of researchers [23–28] performed FSW of aluminum alloys with different tool geometries and tool materials and came with their recommendations for better tool geometry for the given process parameters. A tool with triflute geometry was found better for FSW of 6082-T6 aluminum alloy [23]. Taper cylindrical pin performed better during FSW of IS: 65032 Al alloy [24]. Triangular pin was seen as the most efficient one for FSW of Al5754 [25]. Square pin tool was found better for FSW of AA7075-T651 and AA606 alloys [26]. A triangular pin depicted better performance during the FSW of AA2024-T351 [27]. A flat pin profile tool exhibited improved performance during FSW of commercial Al alloy [28].

A group of researchers have determined a higher tensile strength of an FSW joint with a taper threaded tool pin profile against a taper unthreaded tool. Studies pointed to the reduction of the tensile strength of joints with an increase in temperature and higher microhardness in HAZ and WN with the threaded tool pin profile. The average grain size in the stir zone of FSWed joints was reported to be 54.7–251.7 nm under dry FSW [29–32]. Some studies reported better quality weld with the square tool pin profile against pentagonal, square, hexagonal, and threaded cylindrical tool pin profiles [33]. Kumar and Chander [34] observed better quality of FSWed AA5083 and AA6061 joints with taper threaded tool pin profiles against taper cylindrical and taper square tools. Their study observed the maximum tensile strength and equiaxed grain distribution at a tool rotational speed of 900 rpm and welding speed of 40 mm/min.

The tunnel defects in the microstructure and ductile mode of failure were reported in the dissimilar FSWed joint of AA2024 aluminum alloy and 304 stainless steel [35]. Attempts were made to improve the microstructure and corrosion behavior of FSWed joints using laser shock peeing as post-weld treatment [36]. Khajeh et al. [37] achieved the optimum Ultimate Tensile Strength (UTS) of 142 MPa, a percentage elongation of 5%, and electrical resistivity of 33 nΩm at a tool rotational speed of 948 rpm and welding speed 85 mm/min for FSW of AA2024 aluminum alloy and copper. The microstructure had a large amount of Al_2Cu and Al_4Cu_9 intermetallic brittle compounds. Wang et al. [38] observed higher elastic modulus and nano-hardness at WN and TMAZ for FSW of A7055 aluminum alloy and higher creep resistance at HAZ and TMAZ. Attempts were made to investigate the effect of tool geometry on microstructure evolution, material flow, and mechanical properties of dissimilar FSWed joints [39–41]. The conical threaded tool pin profile was reported as providing better quality welds against the threaded cylindrical and pyramidal tool pin profiles. A representative of 3D images of tool

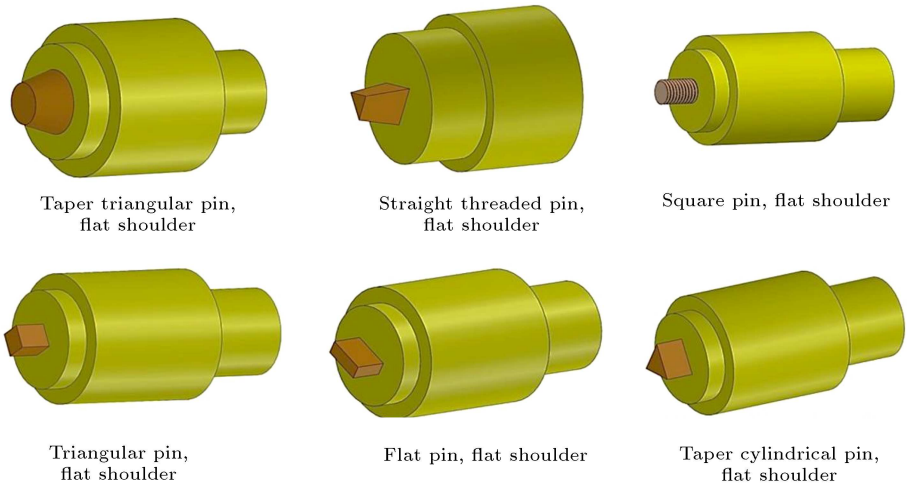

Figure 1. 3D images of different tool geometries used while joining aluminum alloys by FSW.

geometries was used while joining of aluminum alloys by FSW is shown in Figure 1.

Limited studies can be seen on the mechanical properties and fracture behavior of FSWed AA7075-T651 joints considering the influence of process parameters and tool geometry. The present work investigates the mechanical properties, microstructure, and fracture behavior of FSWed AA7075 joints produced with conical threaded and unthreaded pin-type tools. Mechanical properties of FSWed joints are evaluated considering the influence of tool geometry, tool rotation, and welding speed. The material flow in the WN and joint fracture surfaces after the tensile test are investigated based on Scanning Electron Microscopic (SEM) images. The Energy Dispersive X-ray Spectroscopy (EDS) analysis is performed to check the presence of tool debris in the WN.

2. Experimental details

In this study, the AA7075-T651 square butt joints are produced using FSW. Two plates to be welded were initially squared and made free from any burr. Joining of two aluminum plates was kept face-to-face without any gap and firmly clamped during the experiments. FSW experiments were performed on a universal milling machine using conical and conical threaded tools under dry conditions varying with welding speeds (20 and 40 mm/min) and tool rotations (1400 and 2000 rpm). The experimental schematic of FSW is shown in Figure 2 [42,43].

The tools used in the present study having a flat shoulder with a conical pin and a flat shoulder with a conical threaded pin, respectively, are shown in Figure 3(a) and (b). The tool shoulder transfers the axial load on the work surface. The pin stirs and transfers the plasticized material along the joint length. The tool material is H13-type tool steel. The chemical compositions of the tool and workpiece materials are depicted in Tables 1 and 2, respectively. The microstructure of the FSWed joint at different welding zones and the material flow in the WN are studied using optical and SEM images. The EDS

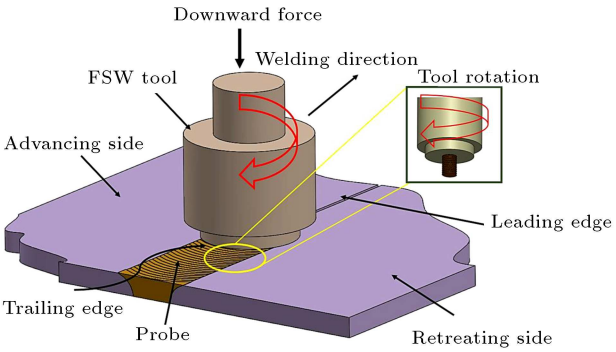

Figure 2. A schematic of FSW process.

Table 1. The chemical composition (% weight) of H13 FSW tool [42,43].

Elements	Cr	Mo	Si	V	C	Ni	Cu	Mn	P	S
%	4.75	1.10	0.80	0.80	0.32	0.3	0.25	0.2	0.03	0.03

Table 2. Chemical composition (% weight) of AA7075-T651 alloy [42,43].

Elements	Si	Fe	Cu	Mn	Mg	Zn	Ni	Pb	Sn	Ti	Cr	Al
%	0.069	0.204	1.64	0.0060	2.33	5.28	0.012	0.012	< 0.0050	0.028	0.195	90.22

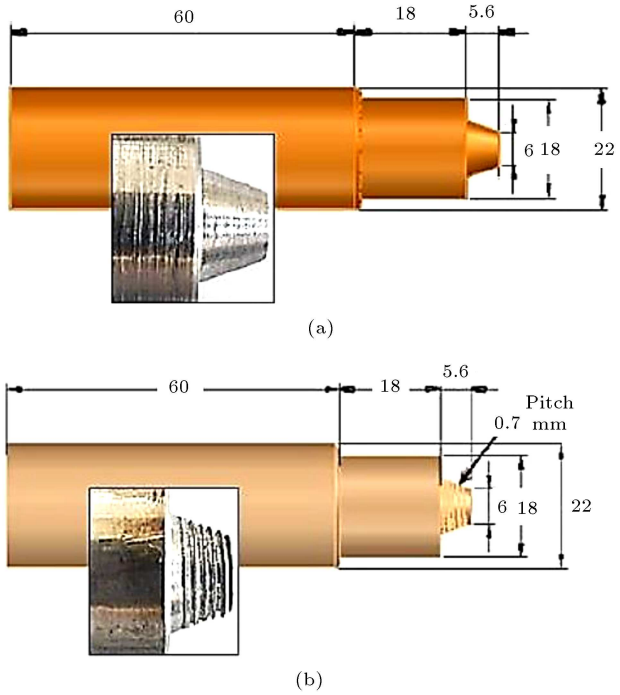

Figure 3. Tool geometries used in FSW: (a) Conical pin type tool and (b) conical threaded pin type tool (all dimensions are in mm) [42-43].

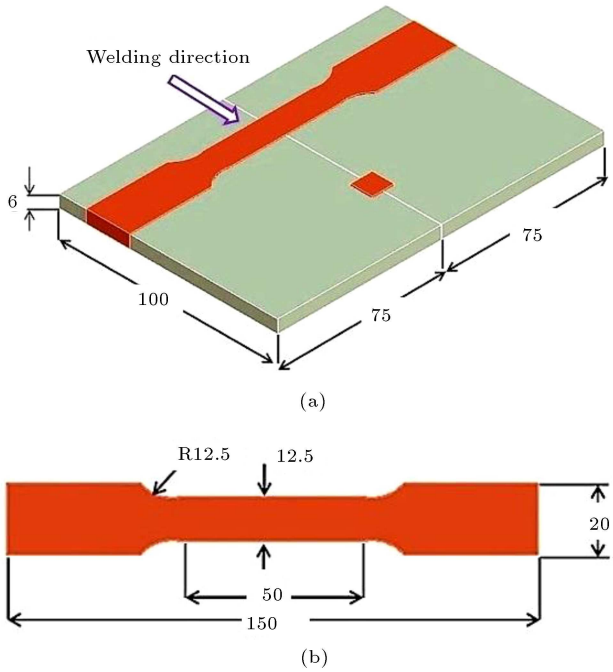

Figure 4. (a) Plate dimensions showing position for extraction of test specimens. (b) Tensile test specimen (all the above-mentioned dimensions are in mm).

analysis is performed to determine the presence of the tool materials in the WN. The mechanical properties of the joints such as the UTS, microhardness in different welding zones (namely WN, TMAZ, HAZ, and BM), and surface roughness are investigated considering the effect of process parameters and tool geometry.

The transverse tensile strength, efficiency, and percentage elongation of the joint were evaluated using a tensile test as per the ASTME8M standard on a universal testing machine. Figure 4(a) and (b) show AA7075 aluminum alloy plate exhibiting the position for extraction of the test specimen and extracted tensile test specimen, respectively. Vicker's microhardness tester was employed to measure the microhardness (at WN, TMAZ, HAZ, and BM) as per the ISO6507 standard using the diamond indenter (136°) with a load of 100 g and a dwell time of 20 seconds. The surface roughness was measured as 25 mm from the start of a weld, in the middle of the weld, and 25 mm before the end of the weld. An average of the three values was taken.

The microstructure of the FSWed joint in different welding zones and the material flow in the WN are studied using a field emission scanning electron microscope. The elemental analysis at WN was performed using EDS in conjunction with SEM images.

3. Results and discussion

In this section, the mechanical properties, microstructure, and fracture behavior of FSWed AA7075 joints are presented and discussed considering the influence of process parameters and tool geometry. The joint efficiency was estimated when using both types of tools. The UTS of the base material obtained after the tensile test was 550 MPa. The experimental matrix with the mechanical properties for the conical pin-type tool (Runs R1 and R2) and conical threaded pin-type tool (Runs R3 and R4) is shown in Table 3.

Table 3. Experimental matrix showing mechanical properties for conical pin and conical threaded pin-type tools.

Run	Tool geometry	Tool rotation (rpm)	Welding speed (mm/min)	Tensile strength (MPa)	Peake longation (%)	Joint efficiency (%)	Surface roughness (μm)
R1	Conical pin	1400	20	65	2	12	18.72
R2	Conical pin	2000	40	20.98	4.1	4	9.59
R3	Conical threaded pin	1400	20	168.83	4.9	31	17.65
R4	Conical threaded pin	2000	40	188	5.7	34	16.15

3.1. Mechanical properties of FSWed joints

Stress-strain curves for FSWed joints produced using the conical pin-type tool (R1 and R2) and conical threaded pin type tool (R3 and R4) are shown in Figure 5. Moreover, Figure 6(a)–(c) show the variation in UTS, microhardness at WN, and surface roughness with respect to processes parameters and tool pin profile, respectively. Figures 5 and 6(a) depict the maximum tensile strength of 188 MPa for the FSWed joint with the conical threaded pin-type tool at a tool rotation of 2000 rpm and a welding speed of 40 mm/min (Run R4). However, the FSWed joint with the maximum tensile strength of 65 MPa can be seen for the conical pin-type tool at a tool rotation of 1400 rpm and a welding speed of 20 mm/min (Run R1).

The tensile strength was observed to increase with the tool rotation for the conical threaded tool pin profile. The temperature considerably increases across the weld samples with the tool rotational speed due to greater frictional effects of the rotating tool on the workpiece. However, with the conical tool pin profile, less frictional heat is generated due to the smaller contact area between the tool pin profile and workpiece; hence, lower tensile strength was observed. The higher tensile strength for FSWed joints with the conical threaded pin-type tool could be attributed to better stirring of the material. The conical threaded pin increased the amount of material, both in transporting per revolution and extruding backward, resulting in more plastic deformation. It causes the fine grain size at the WN, resulting in higher tensile strength for FSWed joints. Similar observations were reported during FSW of AA6101-T6 and AA7075-T651 aluminum alloy with a taper threaded tool pin profile [29–31]. The joint efficiency was determined using the tensile strength and BM strength of the joint. The maximum joint efficiency of 34% can be seen with a conical threaded pin-type tool against 12% with a conical pin-type tool. The FSWed joint produced using a conical threaded pin-type tool sustained maximum tension of 14553 N with peak elongation of 5.7% at a tool rotation of 2000 rpm and welding speed of 40 mm/min against 4.1% with a conical pin-type tool.

The FSWed joint produced with a conical threaded pin-type tool sustained higher tension load with maximum peak elongation. Greater heat input is provided to the welds when using higher tool rotation and welding speed. This causes the dynamic recrystallization of the microstructure, leading to higher elongation. However, weld defects/flaws in the WN and its interfaces with TMAZ were observed for the joint obtained using a conical pin at a higher tool rotation, and welding speed resulted in lower tension load and peak elongation. The analysis of the FSWed joint having better tensile strength and joint efficiency with the conical threaded pin-type tool against the conical pin type tool is discussed with the SEM images at different weld zones in Section 3.2.

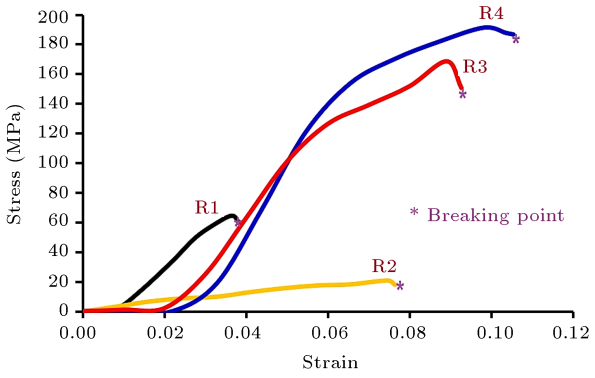

Figure 5. Stress-strain curves for FSW AA7075-T651 joints using conical pin (R1 and R2) and conical threaded pin-type tools (R3 and R4).

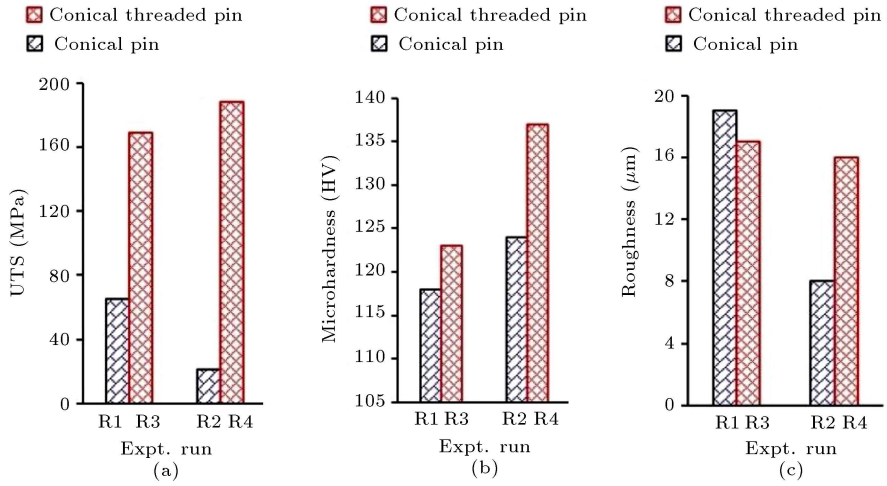

Figure 6. Variation of mechanical properties with processes parameters and tool geometry: (a) UTS, (b) microhardness, and (c) surface roughness.

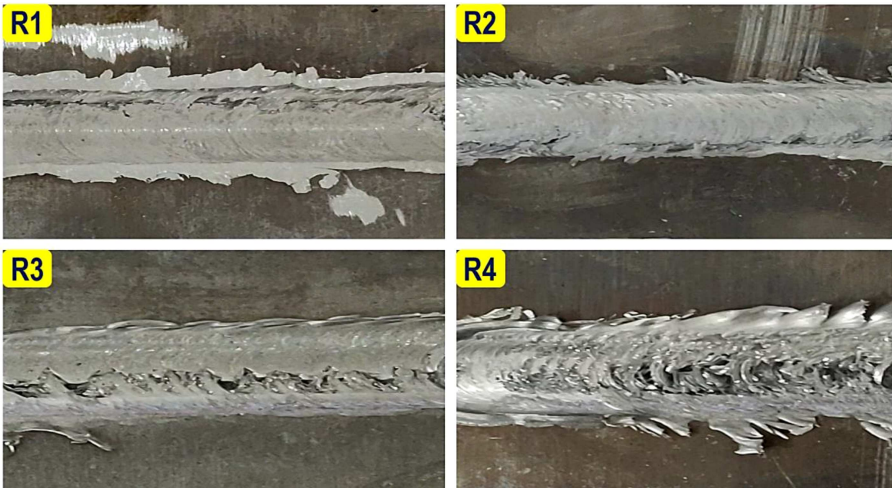

Figure 7. Weld top surface images with the conical pin (R1 and R2) and conical threaded pin (R3 and R4).

The effectiveness of FSW can be assessed by obtaining the surface roughness of the joints. Images of weld top surface are shown in Figure 7. The obtained average surface roughness can be seen in the range of 9 to 19 μm with both tools (Table 3). The lowest surface roughness of 9.59 μm was obtained at a welding speed and a tool rotational speed of 40 mm/min and 2000 rpm, respectively, using the conical pin-type tool (Figure 6(c)). However, significant voids and porosity can be seen in the weld bead at higher values of FSW process parameters with the conical pin-type tool, as shown in Figure 7 marked as R2. Negligible variation in the surface roughness was observed with the FSW process parameters for the conical threaded pin-type tool (Table 3).

The microhardness values of FSWed AA7075-T651 joints were measured at various points from the weld center on both sides of the joint. The variation of microhardness observed in the weld region is shown in Figure 8. Higher plastic deformation and the severe extrusion during FSW cause variation in the grain size and the microhardness in the welded region. The microhardness of FSWed joints exhibited variation in the welding zone, mostly the following distribution of a letter 'W' shape, and was found maximum in the WN and minimum in the HAZ. The marginally higher microhardness values were obtained with a conical threaded pin. It could be attributed to better stirring of the material with threads. The obtained maximum hardness is 137 HV at the WN with the conical threaded pin (Figure 6(b)). It can be seen that the microhardness in WN is higher when the joint is produced using a conical threaded tool pin profile (Runs R3 and R4).

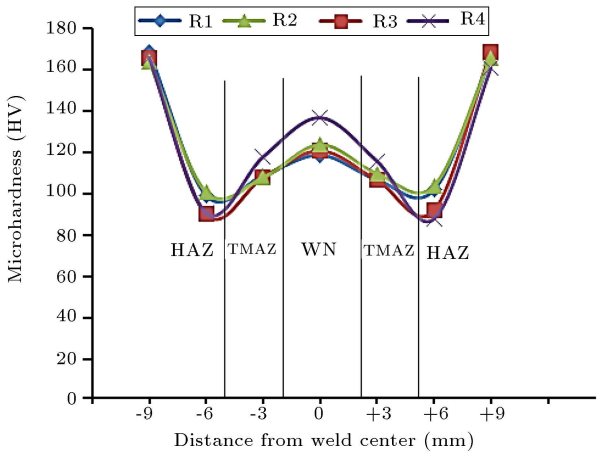

Figure 8. Microhardness variation on both sides of the joint from the weld center.

3.2. Microstructure of FSWed joints

Figure 9 depicts the SEM images of WN, TMAZ, and HAZ of the FSWed joint obtained with the conical pin-type tool at run R1. Large and elongated grains and voids with coarse and heterogeneous grain distribution at WN can be seen in Figure 9(a). Voids observed at WN could be attributed to lower heat generation resulting in instant solidification of the melted material. The grain size can be seen at WN in the range of 3–6 μm.

Figure 9(b) depicts the SEM image of TMAZ at run R1. A large porosity due to the uneven mixing of material can be seen. The coarser and heterogeneously distributed grains than those at WN differentiate this weld region. This weld region is TMAZ which is adjacent to WN. The large voids with circular grains having sizes of 8–13 μm indicate that less heat was transferred from WN to TMAZ. From Figure 9(c), a coarser, elongated, and heterogeneous grain distribution having grain sizes of 13–17 μm, being more than those observed at WN and TMAZ, can be seen. This weld zone is HAZ which is in between the TMAZ and the BM. The higher grain size at HAZ

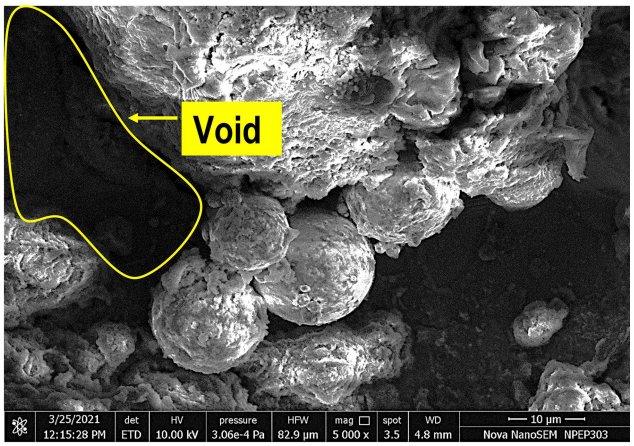

(a)

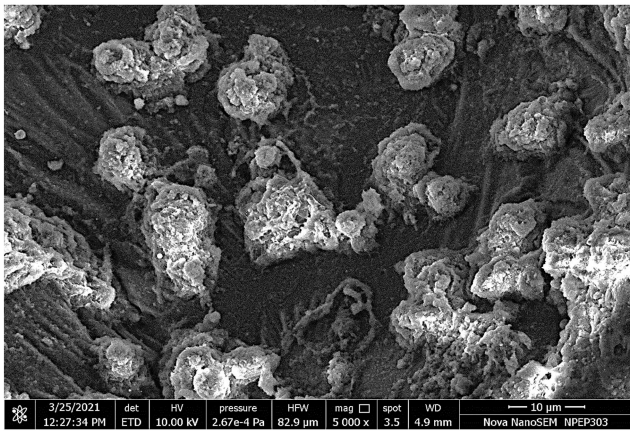

(b)

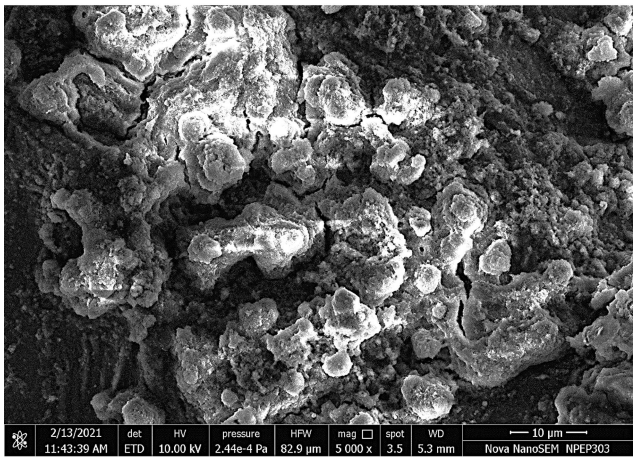

(c)

Figure 9. SEM images at run R1 of: (a) WN, (b) TMAZ, and (c) HAZ.

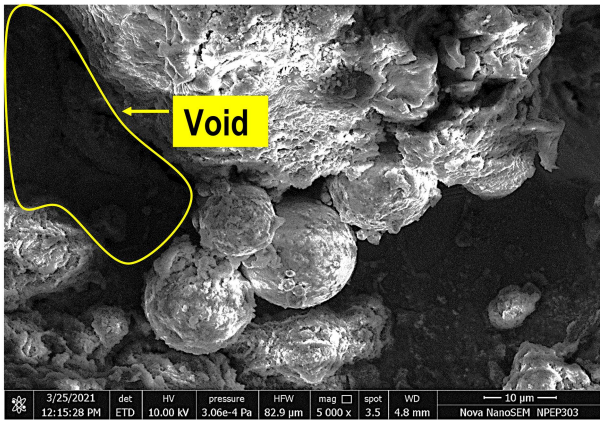

(a)

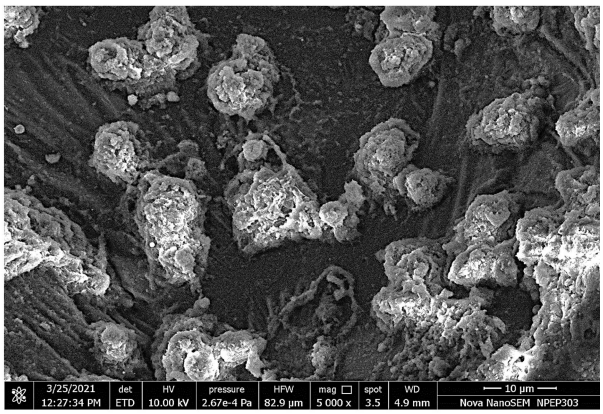

(b)

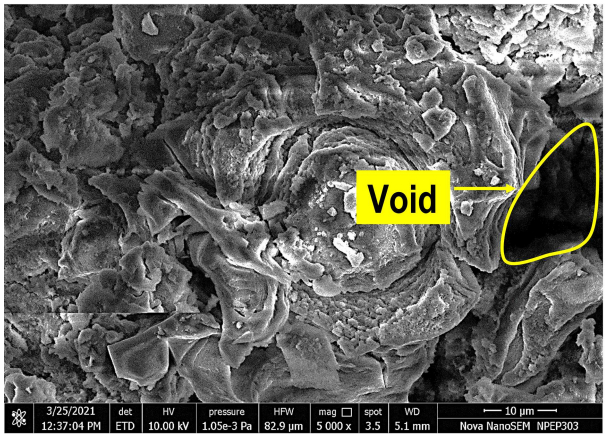

(c)

Figure 10. SEM images at run R2 of: (a) WN, (b) TMAZ, and (c) HAZ.

shows a comparatively low-temperature region than TMAZ and WN. The tunnel defect is observed in HAZ. These microstructure characteristics at run R1 resulted in lower tensile strength for the FSWed joint. It was observed that the microhardness was reduced from the WN to HAZ, which can be attributed to increase in grain size from the WN to HAZ. The highest microhardness value observed at WN was 119 HV, followed by 107 HV at TMAZ and 102 HV at HAZ.

Figure 10 depicts the SEM images of WN, TMAZ, and HAZ of the FSWed joint obtained with the conical pin-type tool at run R2. In Figure 10(a), a large number of porosity defects and large voids can be seen at WN. The grains that can be seen in WN are coarse and unevenly distributed. These porosity defects are the main reason for the lower tensile strength of the FSWed joint with the conical pin-type tool. The grain size in

WN can be seen around 10–14 μm, which is higher than that observed in the WN at run R1. Figure 10(b) depicts the SEM image of TMAZ at a run R2. Larger voids between the grains, heterogeneous distribution of grains, and equiaxed grains with sizes varying in the range of 3–16 μm can be seen. Figure 10(c) shows the SEM image of HAZ at run R2. In HAZ, voids and heterogeneous distribution of grains having sizes in the range of 13–21 μm can be seen.

Overall, the higher grain sizes and larger voids observed in the microstructure at run R2 compared to run R1 resulted in the lower tensile strength for FSWed joint and joint efficiency. This study observes inadequate material mixture due to low plastic material deformation with the conical pin-type tool. This could be attributed to the smaller contact area of the tool with the workpiece. Moreover, the heterogeneously obtained grains distributed in the weld region with the conical pin-type tool. The highest value of microhardness as 124 HV at WN was observed, which can be attributed to the fine grains observed at WN. The comparatively lower microhardness of 110 HV observed at TMAZ can be attributed to coarser grains seen at TMAZ than that at WN. Similarly, among those observed at WN and TMAZ, the lowest microhardness of 104 HV observed at HAZ can be attributed to coarser grains.

Figure 11 depicts the SEM images of WN, TMAZ, and HAZ of the FSWed joint obtained with the conical threaded pin-type tool at run R3. Figure 11(a) depicts uniform material flow, homogeneous mixing of materials, and finer grains with sizes ranging from 625 nm to 4 μm. A tunnel defect and microvoids also can be seen. The equiaxed circular grains are also observed at WN. It is found that the grains at WN are finer than R1 and R2. It could be attributed to higher heat generated at WN due to the larger contact area of the conical threaded pin-type tool than the conical pin-type tool. Higher heat generated causes the dynamic recrystallization of grains at WN, resulting in finer grains [41]. Figure 11(b) shows the SEM image of TMAZ at run R3. Pasty material flow is free of voids and tunnel defect and the homogeneous grain distribution can be seen. At run R3, more heat is generated at WN (compared to run R1 and R2); hence, the heat transferred to TMAZ was adequate, which resulted in a homogeneous distribution of grains of different sizes ranging between 4–8 μm.

A group of researchers have observed an increase in void size upon decreasing temperature and found coarser grains in the HAZ during the FSW of aluminium alloys [1,2]. Lower temperature at the HAZ than that at TMAZ and WN could be attributed to the impact of the frictional heat against the dynamic recrystallization at WN and TMAZ. Rao et al. [7] reported the finer grains at WN than the HAZ in

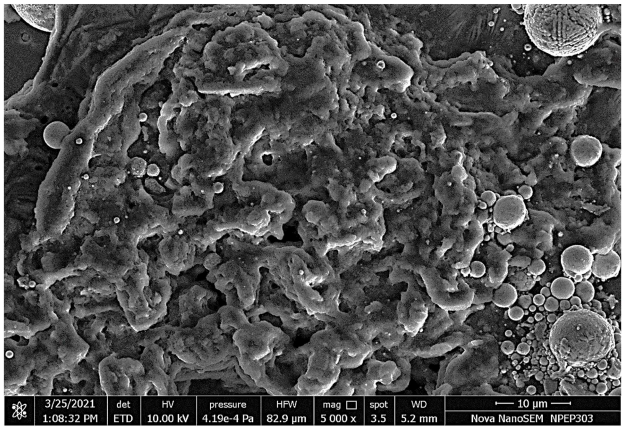

(a)

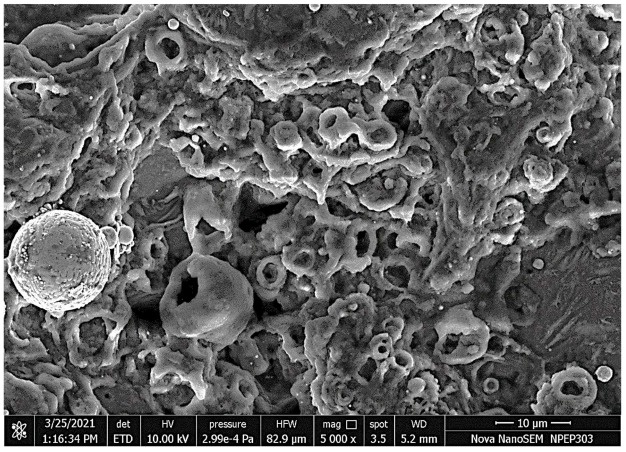

(b)

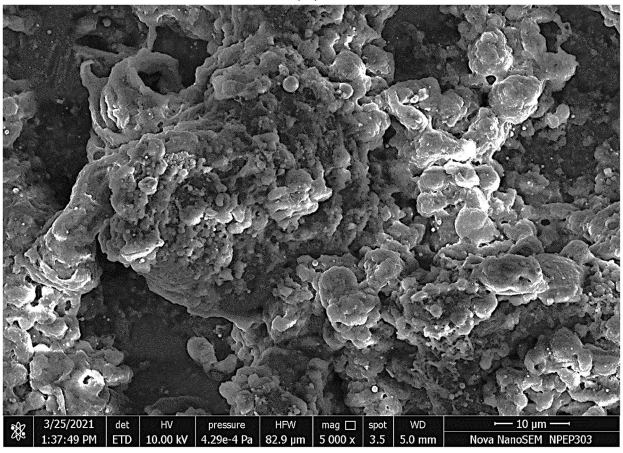

(c)

Figure 11. SEM images at run R3 of: (a) WN, (b) TMAZ, and (c) HAZ.

FSWed AA7075 aluminum alloy. The increase in microhardness at WN improves the grain size at WN.

The present study also detected variation in grain sizes at WN, TMAZ, and HAZ in line with the available literature [1,2,7] and can be confirmed based on the SEM images for conical and conical threaded tool pin profiles.

Figure 11(c) depicts the SEM image of HAZ at

run R3. Homogeneous distribution of grains with a uniform flow of material, the voids, and the elongated grain with the torn edge can be seen. The heat transferred to HAZ from the WN was greater than R1 and R2; hence, homogeneous grain distribution with fewer voids could be seen. The highest microhardness of 121 HV was identified at WN due to finer grains, followed by 108 HV at TMAZ due to the presence of coarser grains than the WN and 100 HV at HAZ due to coarser grains than the WN and TMAZ.

Figure 12 depicts the SEM images of WN, TMAZ, and HAZ of the FSWed joint obtained with the conical threaded pin-type tool at run R4. The proper mixing of the material, the equiaxed grains, with homogeneous distribution of the finer grains having sizes in the range of 600 nm to 2 μm can be seen in Figure 12(a). These favorable microstructure characteristics can be attributed to greater heat generated at a higher tool rotation and a welding speed with the larger contact area of the conical threaded pin-type tool. However, tunnel defects and microvoids can be seen at WN. Figure 12(b) shows the SEM image of TMAZ at run R4. The laminar flow of the material, the equiaxed grains with the homogeneous distribution of grain sizes in the range of 4–7 μm, can be seen with a single tunnel defect. The porosity defects observed in TMAZ with the conical pin-type tool were not seen with the conical threaded pin-type tool. It could be attributed to higher heat transfer from WN to TMAZ at R4 than that at to R1, R2, and R3.

Figure 12(c) depicts the SEM image of HAZ at run R4. The laminar and uniform flow of the material with a tunnel defect can be seen. Moreover, a homogeneous distribution of grains having grain sizes in the range of 6–8 μm can be seen in the HAZ. This could be attributed to the transfer of an adequate amount of heat to HAZ from WN compared to R1, R2, and R3. Proper mixing of the material in the WN, a homogeneous distribution of finer grains, and a joint comparatively free of defects produced the FSWed joint with better tensile strength using the conical threaded pin-type tool. The highest microhardness of 137 HV was observed at WN due to finer grains, followed by 116 HV at TMAZ due to the presence of coarser grains than that at WN as well as 98 HV at HAZ due to coarser grains than those WN and TMAZ.

Beygi et al. [44] reported that the contact area between tool and material played an important role in obtaining quality weld. With increase in the size of the contact area between the tool and the workpiece, the axial load increased and fewer defects were formed due to the higher hydrostatic pressure. Further, the sticking condition increased the shearing contact area between the tool shoulder and material; therefore, a larger quantity of material enters the shear plastic zone to be transferred around the tool. In the present study,

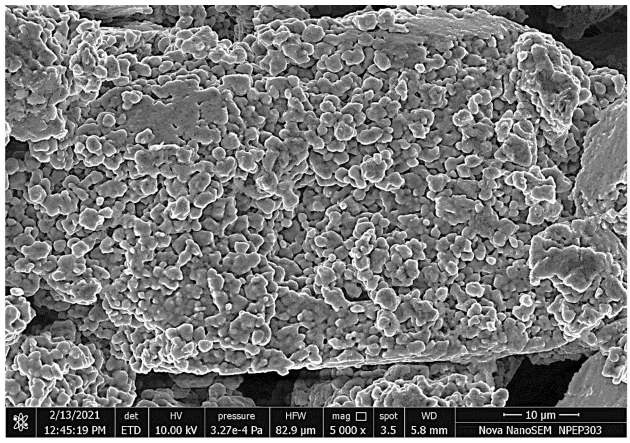

(a)

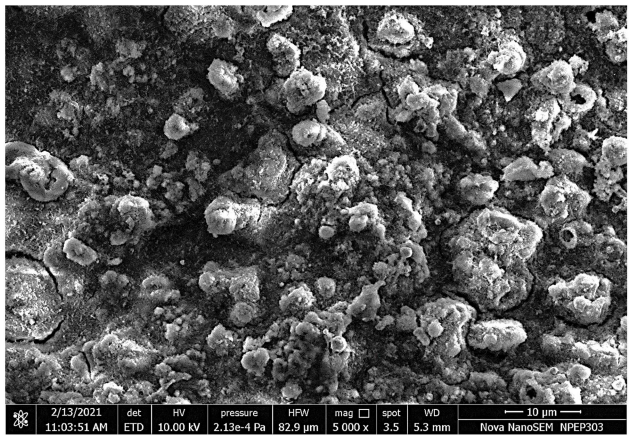

(b)

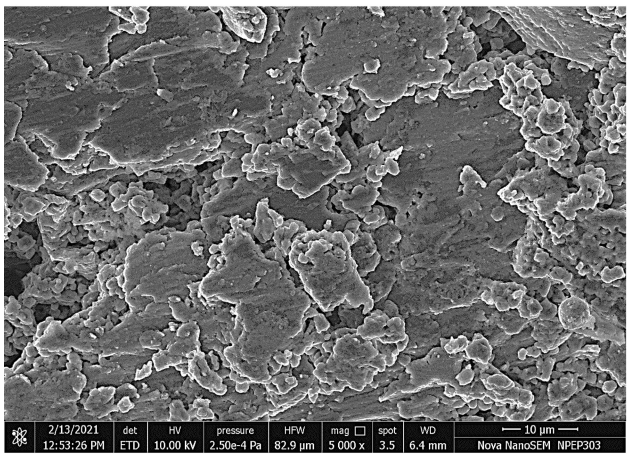

(c)

Figure 12. SEM images at run R4 of: (a) WN, (b) TMAZ, and (c) HAZ.

better results are observed at R3 and R4 using the conical threaded tool pin profile. The conical threaded tool pin profile provided a larger contact area, which resulted in obtaining a finer grained structure in WN, TMAZ, and HAZ than the joints produced by the conical tool pin profile at R1 and R2.

3.3. Fracture behavior of FSWed joints

After the tensile test, the samples were fractured.

Figure 13. Damaged samples for conical and conical threaded tool pin profiles.

Figure 13 depicts the fractured specimens brought side by side. All the FSWed specimens were fractured in the HAZ due to lower microhardness and they exhibited ductile behavior during fracturing. The joints produced with the conical pin-type tool had large voids with varied particles on the fractured surfaces, especially at a higher tool rotation of 2000 rpm and a welding speed of 40 mm/min. On the other hand, fracture surfaces of the joints produced with the conical threaded pin-type tool had a homogeneous distribution. Micro-voids of different sizes and shapes were observed on the fractured surfaces. The fracture behavior of FSWed joints is discussed with the SEM images in Section 3.3.

SEM images of the fractured surface specimens with a conical pin type tool (R1 and R2) and conical threaded pin-type tool (Run R3 and R4) had large-scale equiaxed dimples and tear ridges, indicating the occurrence of fracture in a ductile manner. Figure 14(a) and (b) depict the SEM images of the fractured surfaces of the tensile specimens at R1 and R2, respectively. Broken particles with a small and deep dimple can be seen in Figure 14(a). However, particles getting detached from the weld line and the small dimples along with the torn edges can be seen in Figure 14(b). The dimples are formed by the amalgamation of micro voids that usually begin adjacent to grain boundaries and second-phase particles. The dimple sizes affect the sustaining ability of plastic deformation during tensile testing. The smaller size dimples observed at R1 and R2 indicate lower plastic deformation at the WN with the conical pin-type tool, resulting in lower tensile strength of the FSWed joint at R1 and R2.

Figure 15(a) and (b) depict the SEM image of the fracture surfaces of the specimens after the tensile test at R3 and R4, respectively. Broken, pill-off particles, along with larger dimples, can be seen in Figure 15(a). Also, shallow, large dimples with torn edges can be seen in Figure 15(b). The larger dimples indicate more plastic deformation at WN, leading to

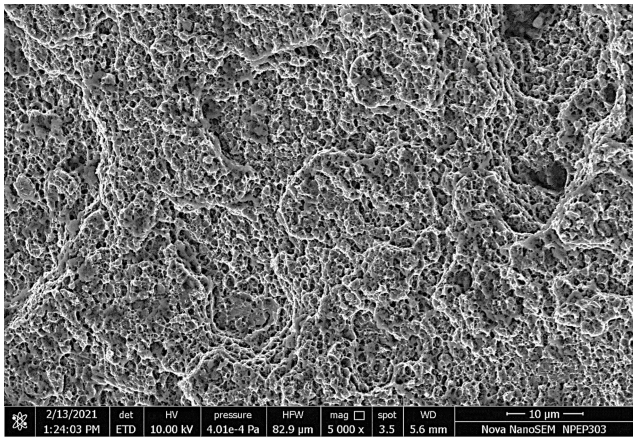

(a)

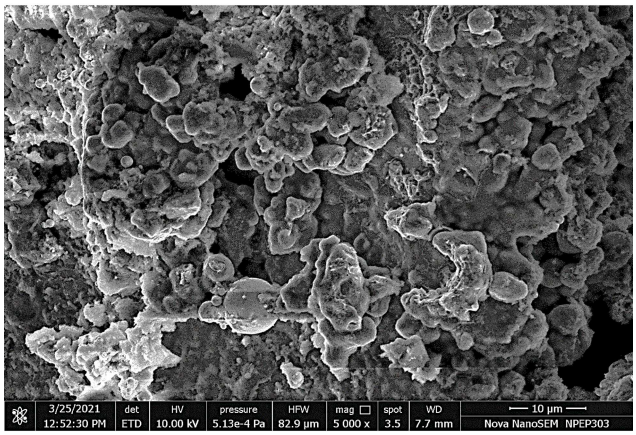

(b)

Figure 14. SEM images of fractured surface at (a) R1 and (b) R2.

better tensile strength for FSWed joints at R3 and R4. However, comparatively more equiaxed, large, and shallow dimples observed at run R4 than those at run R3 produced a higher tensile strength of 188 MPa with the conical threaded pin-type tool. On the other hand, smaller dimples observed at run R2 indicated lower plastic deformation and hence, a lower tensile strength of 20.88 MPa with the conical pin-type tool. The distinct fracture behaviors observed for the FSWed joints can be correlated with the heat generations during the process. The conical threaded pin-type tool generated more heat due to the larger contact area with the workpiece than the conical pin-type tool. The variation in the heat generated in the FSW process affected grain sizes, grain distributions, and defects at HAZ, resulting in different fracture behaviors of FSWed joints [44].

A group of researchers observed failure of the FSWed tensile test specimens at HAZ due to the coarser grains and lower microhardness [2,5–7]. HAZ is a softer region as it experiences less plastic deformation due to lower temperature. The present study observed a decrease in the microhardness with an increase in grain size, which is in line with the Hall-Petch equation.

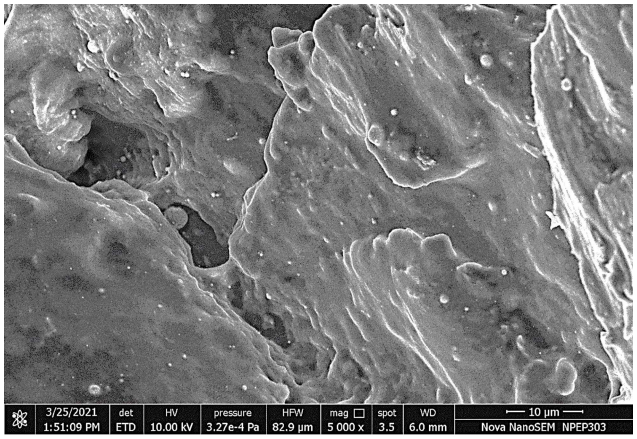

(a)

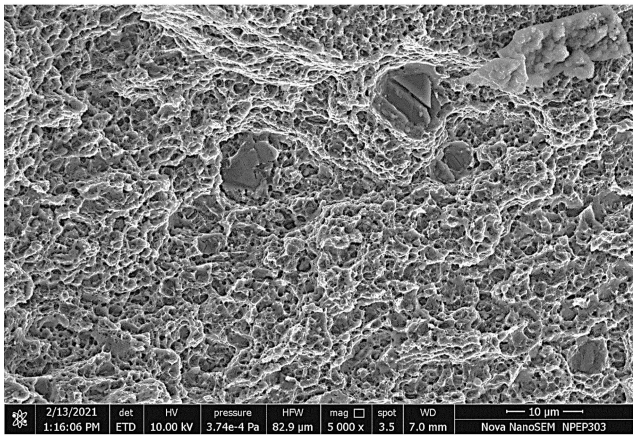

(b)

Figure 15. SEM images of fractured surface at: (a) R3 and (b) R4.

(a)

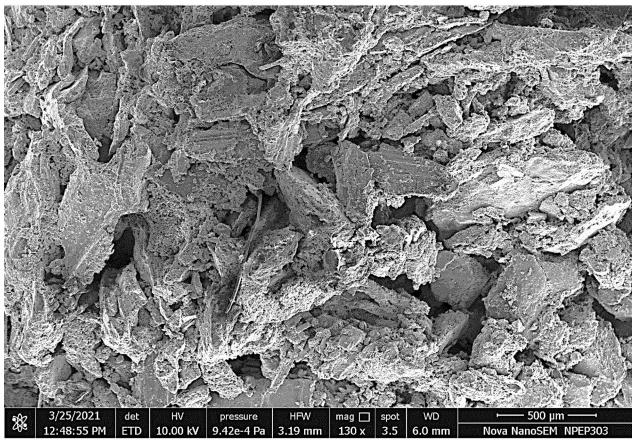

(b)

Figure 16. SEM images showing material flow at: (a) R1 and (b) R2.

The lower microhardness and coarser grains caused a fracture in the FSWed tensile test specimen at HAZ, as seen from the SEM images (Figure 15).

3.4. Material flow and EDS analysis

The weld quality can be determined considering the flow of pasty material beneath the FSW tool. Figures 16 and 17 depict the material flow at WN. Two types of material flow are observed in the present study: Laminar and turbulent.

The turbulent material flow can be seen in Figure 16(a) and (b) for R1 and R2. However, the laminar material flow can be seen in Figure 17(a) and (b) for R3 and R4. The welded microstructure can be seen as free of defects such as cavities and porosity. The joint under turbulent flow conditions were subject to such defects as decreased degree of crystallinity and tunnel appearance. The particles in WN were observed to be distorted and were pulled off from the joining line for runs R1 and R2 with the conical pin-type tool (Figure 16). However, the FSWed joints produced with the conical threaded pin-type tool (Runs R3 and R4) had a more uniform material flow (Figure 17). The FSW experimental analysis showed that the laminar flow and uniform structure gave rise to higher joint strength, joint hardness, and a percentage elongation [43]. Beygi et al. [45] reported a decrease in the number of weld defects at a higher tool rotational speed. The higher temperature generated at a higher tool rotational speed caused better material flow and higher mechanical properties of a weld. In the present study, it was observed that better mechanical properties for a weld were produced at a higher tool rotational speed of 2000 rpm and a welding speed of 40 mm/min (Run R4). However, this impact can be seen as more prominent with the conical threaded pin-type tool due to the larger contact area.

In the present work, the EDS analysis was performed to check the presence of tool debris in the WN for all the FSWed joints obtained at R1 to R4. SEM images of the center of the WN was were captured with EDS analysis for all the FSWed specimens. A representative EDS analysis at the center of the WN (Run R4) with the conical threaded pin-type tool is depicted in Figure 18. The EDS analysis showed no trace of any debris or tool material element in the WN. Mostly, elements such as Mn, Ni, and Cr were seen as getting eliminated from the WN. EDS analysis of the

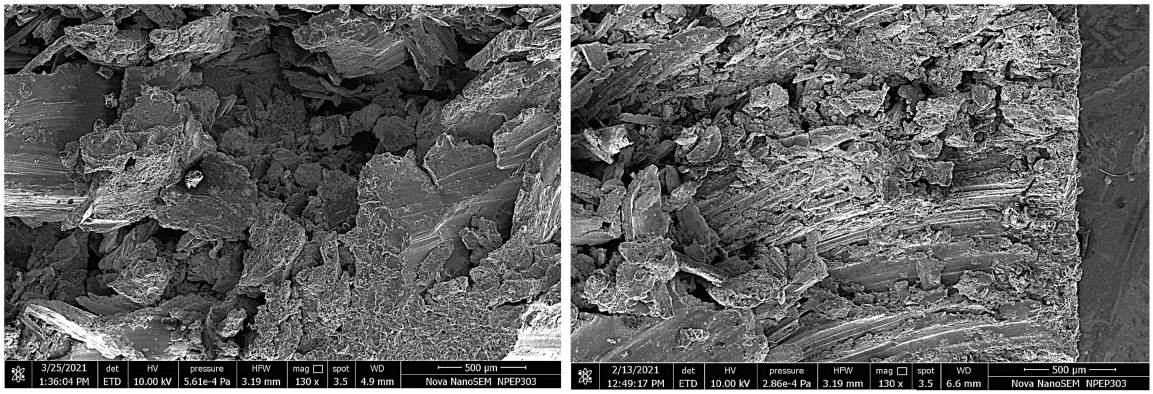

(a) (b)

Figure 17. SEM images showing material flow at (a) R3 and (b) R4.

El	AN	Series	Unn. C (wt. %)	Norm. C (wt. %)	Atom C (wt. %)	Sigma (wt. %)
Al	13	K-series	24.54	53.9	70.35	1.19
Zn	30	L-series	11.1	24.37	13.12	0.79
Cu	29	L-series	3.42	7.51	4.16	0.91
Mg	12	K-series	3.03	6.65	9.64	0.23
Pb	82	M-series	2.13	4.68	0.8	0.2
Fe	26	K-series	0.63	1.39	0.88	0.23
Ti	22	K-series	0.53	1.16	0.85	0.12
Sn	50	L-series	0.11	0.25	0.07	0.06
Si	14	K-series	0.04	0.1	0.12	0.04
Mn	25	K-series	0	0	0	0
Ni	28	L-series	0	0	0	0
Cr	24	K-series	0	0	0	0
Total			28.03	100	100	

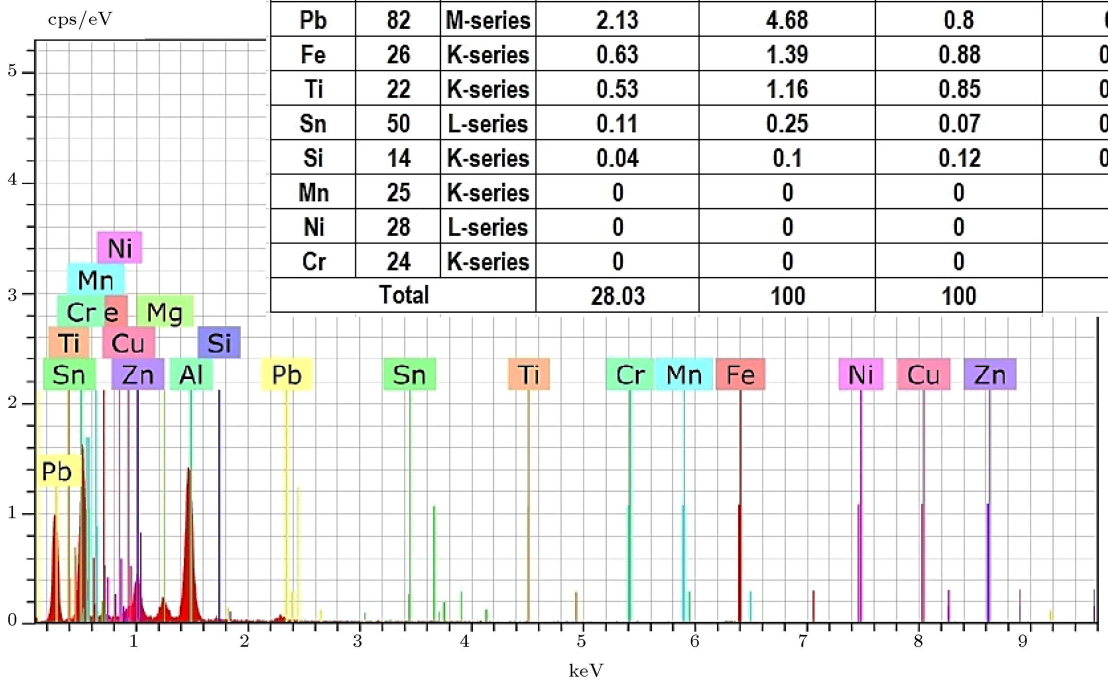

Figure 18. Energy Dispersive X-ray Spectroscopy (EDS) analysis of WN at R4.

FSWed joints showed major wt, a percentage of Al, Cu, Mg, and Zn. The EDS microanalysis demonstrated that the particles in the FSW joint mainly consisted of the $\eta(MgZn_2)$ phase.

The present study finds better mechanical properties, favorable microstructure, and ductile-type fracture behavior with the conical threaded pin-type tool. However, further research is required to optimize the FSW performance with this tool to achieve better tensile strength, microhardness, and minimum surface roughness considering the wide range of tool rotations, welding speeds, and tool plunge depth. Studies are also required to improve the joint efficiency of FSW of AA7075 alloys considering hybrid welding techniques and post-weld treatments.

4. Conclusions

In the present work, mechanical properties,fracture behavior of Friction Stir Welded (FSWed) AA7075

joints were investigated considering the effect of tool geometry and process parameters. FSWed joints were produced using the conical pin and conical threaded pin-type tools with tool rotational speeds of 1400 and 2000 rpm and welding speeds of 20 and 40 mm/min, respectively. The material flow at the Weld Nugget (WN) and joint fracture surfaces after the tensile test were investigated based on Scanning Electron Microscopic (SEM) images. The Energy Dispersive X-ray Spectroscopy (EDS) analysis was performed to check the presence of the tool debris in the WN. The following conclusions could be drawn from the present work:

- The FSWed joint showed higher values of the tensile strength (188 MPa), percentage elongation (5.7%), and microhardness (137 HV) using the conical threaded pin-type tool and at welding and tool rotational speeds of 40 mm/min and 2000 rpm. However, the lower surface roughness of 9.59 μm was obtained with the conical pin-type tool. However, with the application of this tool, higher porosity and voids were observed in the welding zone that substantially lowered the tensile strength of the joint;
- The microhardness of FSWed joints illustrated variation of the welding zone, mostly following the distribution a letter 'W' shape, and was found to be maximum at the WN and minimum at the Heat-Affected Zone (HAZ). Marginally higher microhardness values observed using the conical threaded pin-type tool could be attributed to better material stirring with threads;
- An inadequate material mixing was observed with the conical pin-type tool due to the low plastic deformation of the material. It could be attributed to the smaller contact area of the tool with the workpiece. Moreover, the grains found heterogeneously were distributed in the weld region with the conical pin-type tool. Overall, higher grain sizes and larger voids observed in the microstructure with the conical pin-type tool resulted in the lower joint efficiency and tensile strength for the FSWed joint. However, the proper mixing of the material in the WN, the pasty material flow, the FSWed joint free of voids and tunnel defect, and a homogeneous distribution of finer grains were observed with the conical threaded pin-type tool;
- All the FSWed specimens were fractured at HAZ due to lower microhardness and exhibited ductile behavior during fracturing. The conical pin type tool produced smaller size dimples in the microstructure. It was demonstrated that lower plastic deformation at WN resulted in lower tensile strength of the FSWed joint. However, comparatively equiaxed, large, and shallow dimples in the microstructure obtained with the conical threaded pin-type tool resulted in the higher tensile strength of the FSWed joint. The variation in the heat generated during the Friction Stir Welding (FSW) process affected grain sizes, grain distributions, and defects at HAZ, which led to different fracture behaviors of FSWed joints;
- This study finds scope for more work to improve the joint efficiency of FSW of AA7075 alloys considering hybrid welding techniques and post-weld treatments.

References

1. Cetkin, E., Çelik, Y.H., and Temiz, S. "Microstructure and mechanical properties of AA7075/AA5182 jointed by FSW", *J. Mater. Process. Technol*, **268**, pp. 107–116 (2019).
2. Sharma, C., Dwivedi, D.K., and Kumar, P. "Effect of welding parameters on microstructure and mechanical properties of friction stir welded joints of AA7039 aluminum alloy", *Mater. Des*, **36**, pp. 379–390 (2012).
3. Szklarska-Smialowska, Z. "Pitting corrosion of aluminum", *Corros. Sci.*, **41**, pp. 1743–1767 (1999).
4. Nosko, M., Štepánek, M., Zifčák, P., et al. "Solid-state joining of powder metallurgy Al-Al_2O_3 nanocomposites via friction-stir welding: Effects of powder particle size on the weldability, microstructure, and mechanical property", *Mater. Sci. Eng. A.*, **754**, pp. 190–204 (2019).
5. Zhang, C., Cao, Y., Huang, G., et al. "Influence of tool rotational speed on local microstructure, mechanical and corrosion behavior of dissimilar AA2024/7075 joints fabricated by friction stir welding", *J. Manuf. Process*, **49**, pp. 214–226 (2020).
6. Zhang, J., Upadhyay, P., Hovanski, Y., et al. "High-speed friction stir welding of AA7075-T6 sheet: Microstructure, mechanical properties, micro-texture, and thermal history", *Metall. Mater. Trans. A Phys. Metall. Mater. Sci*, **49**, pp. 210–222 (2018).
7. Rao, T.S., Reddy, G.M., and Rao, S.R.K. "Microstructure and mechanical properties of friction stir welded AA7075-T651 aluminum alloy thick plates", *Trans. Nonferrous Met. Soc. China (English Ed.)*, **25**, pp. 1770–1778 (2015).
8. Elatharasan, G. and Kumar, V.S.S. "Corrosion analysis of friction stir-welded aa 7075 aluminium alloy", *Stroj. Vestnik/Journal Mech. Eng*, **60**, pp. 29–34 (2014).
9. Rao, T.S., Rao, S.R.K., and Reddy, G.M. "Microstructure and fracturing behavior of AA7075–T651 aluminum alloy cooled during friction stir welding", *Met. Sci. Heat Treat*, **61**, pp. 379–386 (2019).
10. Ipekoğlu, G., Kiral, B.G., Erim, S., et al. "Investigation of the effect of temper condition on the friction-stir weldability of AA7075 Al-alloy plates", *Mater. Tehnol*, **46**, pp. 627–632 (2012).

11. Barbini, A., Carstensen, J., and Santos, J.F. dos. "Influence of a non-rotating shoulder on heat generation, microstructure and mechanical properties of dissimilar AA2024/AA7050 FSW joints", *J. Mater. Sci. Technol*, **34**, pp. 119–127 (2018).
12. Chen, S., Li, X., Jiang, X., et al. "The effect of microstructure on the mechanical properties of friction stir welded 5A06 Al Alloy", *Mater. Sci. Eng. A*, **735**, pp. 382–393 (2018).
13. Chen, H., Fu, L., and Liang, P. "Microstructure, texture and mechanical properties of friction stir welded butt joints of 2A97 Al-Li alloy ultra-thin sheets", *J. Alloys Compd*, **692**, pp. 155–169 (2017).
14. Azeez, S.T. and Akinlabi, E.T. "Effect of processing parameters on microhardness and microstructure of a double-sided dissimilar friction stir welded aa6082-t6 and aa7075-t6 aluminum alloy", *Mater. Today Proc*, **5**, pp. 18315–18324 (2018).
15. Chinchanikar, S., Gharde, S., and Gadge, M. "Investigation of tool forces, weld bead micro-hardness and surface roughness during friction stir welding of aluminium 6063 alloy", *Adv. Mater. Process. Technol.*, **8**, pp. 1–9 (2020).
16. Kumar, P.V., Reddy, G.M., and Rao, K.S. "Microstructure and pitting corrosion of armor grade AA7075 aluminum alloy friction stir weld nugget zone – Effect of post weld heat treatment and addition of boron carbide", *Def. Technol*, **11**, pp. 166–173 (2015).
17. Kumar, P.S. and Chander M.S. "Effect of tool pin geometry on FSW dissimilar aluminum alloys - (AA5083 & AA6061)", *Mater. Today Proc*, **39**, pp. 472–477 (2020).
18. Mastanaiah, P., Sharma, A., and Reddy, G.M. "Role of hybrid tool pin profile on enhancing welding speed and mechanical properties of AA2219-T6 friction stir welds", *J. Mater. Process. Technol*, **257**, pp. 257–269 (2018).
19. Amirafshar, A. and Pouraliakbar, H. "Effect of tool pin design on the microstructural evolutions and tribological characteristics of friction stir processed structural steel", *Meas. J. Int. Meas. Confed*, **68**, pp. 111–116 (2015).
20. Beygi, R., Mehrizi, M.Z, Verdera, D., et al. "Influence of tool geometry on material flow and mechanical properties of friction stir welded Al-Cu bimetals", *J. Mater. Process. Technol*, **255**, pp. 739–748 (2018).
21. Kumar, K., Kailas, S.V., and Srivatsan, T.S. "Influence of tool geometry in friction stir welding", *Mater. Manuf. Process*, **23**, pp. 188–194 (2008).
22. Banik, A., Saha, A., Barma, J.D., et al. "Determination of best tool geometry for friction stir welding of AA 6061-T6 using hybrid PCA-TOPSIS optimization method", *Meas. J. Int. Meas. Confed*, **173**, p. 108573 (2021).
23. Krasnowski, K., Hamilton, C., and Dymek, S. "Influence of the tool shape and weld configuration on microstructure and mechanical properties of the Al 6082 alloy FSW joints", *Arch. Civ. Mech. Eng*, **15**, pp. 133–141 (2015).
24. Rao, M.S.S., Kumar, B.V.R.R., and Hussain, M.M. "Experimental study on the effect of welding parameters and tool pin profiles on the IS:65032 aluminum alloy FSW joints", *Mater. Today Proc.*, **4**, pp. 1394–1404 (2017).
25. Badarinarayan, H., Shi, Y., Li, X., et al. "Effect of tool geometry on hook formation and static strength of friction stir spot welded aluminum 5754-O sheets", *Int. J. Mach. Tools Manuf*, **49**, pp. 814–823 (2009).
26. Yuvaraj, K.P., Varthanan, P.A., Haribabu, L., et al. "Optimization of FSW tool parameters for joining dissimilar AA7075-T651 and AA6061 aluminium alloys using Taguchi Technique", *Mater. Today Proc*, **45**(2), pp. 919–925 (2020). https://doi.org/10.1016/j.matpr.2020.02.942
27. John, J., Shanmughanatan, S.P., and Kiran, M.B. "Effect of tool geometry on microstructure and mechanical properties of friction stir processed AA2024-T351 aluminium alloy", *Mater. Today Proc*, **5**, pp. 2965–2979 (2018).
28. Suri, A. "An improved FSW tool for joining commercial aluminum plates", *Procedia Mater. Sci*, **6**, pp. 1857–1864 (2014).
29. Abolusoro, O.P. and Akinlabi, E.T. "Experimental investigations of tool pin geometry and process parameter influence on mechanical property of friction stir welded 6101-T6 and 7075-T651 aluminium alloys", *Journal of Physics: Conference Series*, **1378**, pp. 1–9 (2019).
30. Abolusoro, O.P., Akinlabi, E.T., and Kailas, S.V. "Tool rotational speed impact on temperature variations, mechanical properties and microstructure of friction stir welding of dissimilar high-strength aluminium alloys", *J. Brazilian Soc. Mech. Sci. Eng*, **42**, p. 176 (2020).
31. Abolusoro, O.P., Akinlabi, E.T., and Kailas, S.V. "Impact of tool profile on mechanical behavior and material flow in friction stir welding of dissimilar aluminum alloys", *Materwiss. Werksttech*, **51**, pp. 725–731 (2020).
32. Pouraliakbar, H., Beygi, R., Fallah, V., et al. "Processing of Al-Cu-Mg alloy by FSSP: Parametric analysis and the effect of cooling environment on microstructure evolution", *Mater. Lett*, **308**, pp. 1–5 (2022). DOI: 10.1016/j.matlet.2021.131157
33. Goyal, A. and Garg, R.K. "Modeling and optimization of friction stir welding parameters in joining 5086 H32 aluminium alloy", *Sci. Iran*, **26**, pp. 2407–2417 (2019).
34. Kumar, P.S. and Chander, M.S. "Effect of tool pin geometry on FSW dissimilar aluminum alloys - (AA5083 & AA6061)", *Mater. Today Proc*, **39**, pp. 472–477 (2020).
35. Jabraeili, R., Jafarian, H.R., Khajeh, R., et al. "Effect of FSW process parameters on microstructure and mechanical properties of the dissimilar AA2024 Al

alloy and 304 stainless steel joints", *Mater. Sci. Eng. A.*, **814**, pp. 1–13 (2021).

36. Liu, P., Sun, S., and Hu, J. "Effect of laser shock peening on the microstructure and corrosion resistance in the surface of weld nugget zone and heat-affected zone of FSW joints of 7050 Al alloy", *Opt. Laser Technol*, **112**, pp. 1–7 (2019).
37. Khajeh, R., Jafarian, H.R., Seyedein, S.H., et al. "Microstructure, mechanical and electrical properties of dissimilar friction stir welded 2024 aluminum alloy and copper joints", *J. Mater. Res. Technol*, **14**, pp. 1945–1957 (2021).
38. Wang, W., Yuan, S., Qiao, K., et al. "Microstructure and nanomechanical behavior of friction stir welded joint of 7055 aluminum alloy", *J. Manuf. Process*, **61**, pp. 311–321 (2021).
39. Xu, Y., Ke, L., Mao, Y., et al. "Interfacial microstructure evolution of thick plate Al/Mg FSW: Effect of pin size", *Mater. Charact*, **174**, pp. 1–7 (2021).
40. Beygi, R., Mehrizi, M.Z., Verdera, D., et al. "Influence of tool geometry on material flow and mechanical properties of friction stir welded Al-Cu bimetals", *J. Mater. Process. Technol*, **255**, pp. 739–748 (2018).
41. Chinchanikar, S. and Gaikwad, V.S. "State of the art in friction stir welding and ultrasonic vibration-assisted friction stir welding of similar/dissimilar aluminum alloys", *J. Comput. Appl. Res. Mech. Eng*, **11**(1), pp. 67–100 (2021).
42. Gaikwad, V.S. and Chinchanikar, S. "Investigation on surface roughness, ultimate tensile strength, and microhardness of friction stir welded AA7075-T651 joint", *Mater. Today Proc*, **46**(17), pp. 8061–8065 (2021).
43. Gaikwad, V.S. and Chinchanikar, S. "Mechanical behaviour of friction stir welded AA7075-T651 joints considering the effect of tool geometry and process parameters", *Advan. in Mate. & Proce. Techno.* 10.1080/2374068X.2021.1976554
44. Beygi, R., Kazeminezhad, M., Mehrizi, M.Z., et al. "Friction stir butt welding of Al-Cu bilayer laminated composites: analysis of force, torque, and temperature", *Int. J. Adv. Manuf. Technol*, **88**, pp. 393-400 (2017).
45. Beygi, R., Kazeminezhad, M., and Kokabi A.H. "Microstructural evolution and fracture behavior of friction-stir-welded Al-Cu laminated composites", *Meta. and Mate.s Trans. A.*, **45A.**, pp. 361–370 (2014).

Biographies

Vaibhav Subhash Gaikwad is a PhD candidate in the Department of Mechanical Engineering at Vishwakarma Institute of Information Technology, India. He received his MS degree from the Symbiosis International University and BS degree from Pune University. His main research interest is in joining processes. He has published two Patents, one Copyright and 12+ papers in International Journals and Conferences.

Satish Chinchanikar is currently working as a Professor in the Department of Mechanical Engineering at Vishwakarma Institute of Information Technology, India. He received his PhD from the Indian Institute of Technology Kanpur and his MS from Pune University. His main research interest is in advanced manufacturing processes and the machining of hard alloys using coated tools. He has 25+ years of teaching and Industry experience and published 100+ papers in International Journals and Conferences. He has authored a book chapter on the finish machining of hardened steels published by Elsevier and two textbooks on Advanced Manufacturing Processes. He has been awarded an excellent paper certificate at International Conference on Key Engineering Materials in Malaysia. He is working as a reviewer of many peer-reviewed International Journals. He has received 1300+ citations for his work and published several Patents and Copyrights . He strongly believes that teaching and research should go hand in hand.